Isotropic and anisotropic spin-spin interactions and a quantum phase transition in a dinuclear Cu(II) compound

Lia M. B. Napolitano and Otaciro R. Nascimento[*]

Grupo de Biofísica Molecular Sergio Mascarenhas, Departamento de Física e Informática, Instituto de Física de São Carlos, Universidade de São Paulo, Caixa Postale 369, CEP 13560-970, São Carlos, São Paulo, Brazil

Santiago Cabaleiro and Jesús Castro
Departamento de Química Inorgánica, Universidad de Vigo, 36200 Vigo, Spain

Rafael Calvo
Departamento de Física, Facultad de Bioquímica y Ciencias Biológicas, Universidad Nacional del Litoral and INTEC (CONICET-UNL), Güemes 3450, 3000 Santa Fe, Argentina

We report electron-paramagnetic resonance (EPR) studies at $\sim$9.5 GHz (X band) and $\sim$34 GHz (Q band) of powder and single-crystal samples of the compound $Cu_2[TzTs]_4$ [N-thiazol-2-yl-toluenesulfonamidatecopper(II)], $C_{40}H_{36}Cu_2N_8O_8S_8$, having copper(II) ions in dinuclear units. Our data allow determining an antiferromagnetic interaction $J_0=(-113\pm1)$ cm^{-1} ($\mathcal{H}_{ex}=-J_0\mathbf{S_1}\cdot\mathbf{S_2}$) between Cu(II) ions in the dinuclear unit and the anisotropic contributions to the spin-spin coupling matrix $\mathcal{D}$ ($\mathcal{H}_{ani}=\mathbf{S_1}\cdot\mathcal{D}\cdot\mathbf{S_2}$), a traceless symmetric matrix with principal values $\mathcal{D}/4=(0.198\pm0.003)$ cm^{-1} and $\mathcal{E}/4=(0.001\pm0.003)$ cm^{-1} arising from magnetic dipole-dipole and anisotropic exchange couplings within the units. In addition, the single-crystal EPR measurements allow detecting and estimating very weak exchange couplings between neighbor dinuclear units, with an estimated magnitude $|J'|=(0.060\pm0.015)$ cm^{-1}. The interactions between a dinuclear unit and the "environment" of similar units in the structure of the compound produce a spin dynamics that averages out the intradinuclear dipolar interactions. This coupling with the environment leads to decoherence, a quantum phase transition that collapses the dipolar interaction when the isotropic exchange coupling with neighbor dinuclear units equals the magnitude of the intradinuclear dipolar coupling. Our EPR experiments provide a new procedure to follow the classical exchange-narrowing process as a shift and collapse of the line structure (not only as a change of the resonance width), which is described with general (but otherwise simple) theories of magnetic resonance. Using complementary procedures, our EPR measurements in powder and single-crystal samples allow measuring simultaneously three types of interactions differing by more than three orders of magnitude (between 113 cm^{-1} and 0.060 cm^{-1}).

PACS number(s): 76.30.−v

I. INTRODUCTION

The phenomenon of exchange narrowing, first suggested by Gorter and Van Vleck[1] and demonstrated by Van Vleck[2] at dawn of the magnetic-resonance techniques, was nicely described by Anderson and Weiss.[3] Exchange interactions cannot broaden a paramagnetic resonance line because they commute with the components of the magnetic moment. However, they produce a dynamics of the spin system that averages out magnetic dipolar interactions, thus narrowing the line.[4] The "random frequency modulation" model of Anderson and Weiss[3] and Anderson[4] provides a simple but detailed explanation that predicts the effect of the exchange coupling in the magnetic-resonance line widths. These ideas were widely supported by experiments and by other theories,[5–7] and are reviewed in magnetic-resonance textbooks.[8–14] Advances in the Anderson–Kubo theories have been recently reviewed.[15]

Dinuclear units of metal ions are the simplest coupled spin systems. In most cases the exchange couplings between the spins are much larger than the dipolar couplings. Since the discovery of the properties of copper acetate dihydrate by Bleaney and Bowers[16] in 1952, thousands of molecular based magnetic clustered materials (dinuclear and polynuclear) have been reported.[17] Their behaviors have been characterized by a wide variety of experimental techniques with results supporting a fruitful field for theoretical advances and applications. Dinuclear units of metal ions provided a starting point for the great interdisciplinary efforts expended by physicists, chemists, and material scientists in the search of single-molecule magnets (smm).[18] They are also important in bioinorganic chemistry because of their relevance to metal-ion enzymes,[19–21] and considerable efforts have been made in that direction.

The field of molecular magnetic materials is growing very fast, provides a basic understanding of the problems, and very important progress has been made in designing and preparing new smm with specific magnetic properties.[17,18] EPR has played important roles in this progress.[12,16] A goal of most studies of dinuclear and polynuclear units is to understand the relation between the magnetic interactions and the magnetic response and with the molecular structure. Undoubtedly, the magnetic response of polynuclear units depends on their magnetic isolation, which may be characterized by the ratio between the magnetic couplings between neighbor units and that within the unit. This ratio determines

characteristics of the static and dynamic responses and the quality of the unit for applications as a smm or as a model system. It is important to emphasize that there is not a single value for the interaction, but a distribution of values corresponding to pairs of units at different distances. Thus, because of the approximate exponential dependence with distance of the couplings, the standard approximation is to consider the value corresponding to nearest-neighbor units. In most cases the couplings between units are estimated from static susceptibility data using the molecular-field approximation, an approximate method considering the deviations of the observed magnetic behavior from that expected for noninteracting polynuclear units.[17,22] These deviations are usually strongly dependent on experimental uncertainties of the magnetic measurements and on the quality of the sample. Thus, the evaluation of weak interactions acting simultaneously with much stronger interactions is not normally accurate.

Herein we study the dinuclear copper(II) compound named Cu$_2$[TzTs]$_4$ {*N*-thiazol-2-yl-toluenesulfonamidate copper(II) [having 3*d* (Ref. 9) electronic configuration], where TzTs=N-thiazol-2-yl-toluenesulfonamidate, C$_{40}$H$_{36}$Cu$_2$N$_8$O$_8$S$_8$}, reported in Ref. 23. We performed electron-paramagnetic resonance (EPR) experiments at ~9.4 GHz (*X* band) and ~34.5 GHz (*Q* band) in oriented single crystals and in powdered samples within a wide temperature range. These EPR data allow evaluating the isotropic and anisotropic interactions between the copper spins in the dinuclear unit. Most important, our single-crystal measurements allow following the transition of the dinuclear unit from a phase where the anisotropic spin-spin interaction (mainly dipole-dipole coupling) is clearly resolved, to a situation where this interaction collapses as a consequence of the weak exchange interactions with an "environment" of identical units. This is a temperature-independent quantum phase transition leading to a decoherence of the spins in a dinuclear unit, produced by this environment when the center of the random distribution of exchange interactions with neighboring units equals the magnitude of the intradinuclear dipolar coupling. In our single-crystal experiments we move through this transition by carefully varying the orientation of the applied field (and thus the position of the energy levels) in a narrow angular range around the magic angles, where the dipolar interaction is small. Using this new procedure we follow the collapse in the energy space of the dipolar interaction within the dinuclear unit, produced by random exchange interactions with similar neighbor dinuclear units. This phenomenon has not been observed before for electronic spins and allows evaluating the very weak interdinuclear exchange coupling producing the spin dynamics that collapses the intradinuclear anisotropic interactions. The observations are explained in terms of the theories of Anderson and Weiss[3,4] and Kubo and Tomita[5–7] and offer a clarifying experimental view of the classical phenomenon of exchange narrowing.[1–4] It is noteworthy to say that exchange narrowing has been for fifty years one of the most important examples used to build the nonequilibrium thermodynamics and statistical mechanics.[6,7,24] The values of the intradinuclear interactions are compared with previous findings in similar dinuclear units. The quantum phase transition[25] may

be compared with EPR results for mononuclear spin systems in rotated crystal sites,[26–28] for nuclear spins observed in CW NMR experiments,[29] and in the time domain in pulsed NMR experiments.[30,31] Recently Pastawski[32] described other physical systems undergoing similar transitions.

In recent years several important investigations about interacting smm have been reported.[33–36] These works use mainly magnetic (thermodynamic) techniques to obtain information about the effect of these interactions in quantum tunneling and coherence of the spin states. Our EPR measurements in the simpler dinuclear units show how resonant techniques may be helpful in this direction in cases when appropriate single-crystal samples of more complex smm are available.

II. STRUCTURAL DESCRIPTION OF Cu$_2$[TzTs]$_4$

The synthesis, crystallization, chemical properties, and x-ray crystal structure of the compound Cu$_2$[TzTs]$_4$, C$_{40}$H$_{36}$Cu$_2$N$_8$O$_8$S$_8$, where TzTs=N-thiazol-2-yl-toluenesulfonamidate was described in Ref. 23 and we briefly repeat some of these findings. It crystallizes in the monoclinic space group $P2_1/c$ with lattice parameters a=17.389 Å, b=16.300 Å, c=18.368 Å, $\alpha=\gamma=90°$, $\beta=114.364°$, and Z=4 molecules in the unit cell as observed at 293 K. The molecular structure of Cu$_2$[TzTs]$_4$ consists of noncentrosymmetric dinuclear units with chemically different Cu(II) ions, Cu^1 and Cu^2, having fractional coordinates $[x,y,z]$ ≡[0.22269, 0.38661, 0.15272] and [0.28696, 0.37838, 0.31882], respectively.[23] Each copper ion occurs in a slightly distorted square-pyramidal coordination, with four equatorial *N* ligands at about 2 Å and an apical O ligand at 2.729 Å for Cu^1 and at 2.723 Å for Cu^2. Figure 1(a) displays an ORTEP (Ref. 37) view of the molecular structure of Cu$_2$[TzTs]$_4$ including the labels of the most relevant atoms. A simplified sketch of the unit cell of Cu$_2$[TzTs]$_4$ emphasizing the symmetry operations relating the four dinuclear units (labeled A≡[x,y,z], B≡[$-x,1/2+y,1/2-z$], C≡[$-x,-y,-z$], and D≡[$x,1/2-y,1/2+z$]) is displayed in Fig. 1(b). Molecules A and B are related by a 180° rotation around the *b* axis plus a displacement of [0 1/2 1/2]. Molecules C and D are obtained from molecules A and B by inversion operations. The Cu^1-Cu^2 bond distance in the dinuclear units, at 293 K, is 2.786 Å and the metal ions are bridged by four N-C-N bonds at about 90°. As shown by Fig. 1(b), the Cu^1-Cu^2 directions in the four units are nearly parallel to the $c^*=a \times b$ axis.

Figure 2(a) describes relevant chemical paths connecting neighboring dinuclear units.

(i) Cu^1 and Cu^2 ions in neighbor copper dinuclear units A-B at 11.744 Å are connected by an equatorial-equatorial path containing nine diamagnetic atoms, labeled I in Fig. 2(a),

CuA^1-NA-CA-CA-HB$\cdots$CB-CB-CB-SB-NB-CuB^2

including a weak hydrogen bond between a carbon **CA** belonging to molecule type A, acting as a donor, with a carbon **CB** acting as an acceptor, with distances **CA-HB** 2.843 Å and **HB$\cdots$CB** 0.930 Å and the angle **CA-HB$\cdots$CB** is 158.05° (see Refs. 38 and 39 for C-H$\cdots$C bonds). Due to
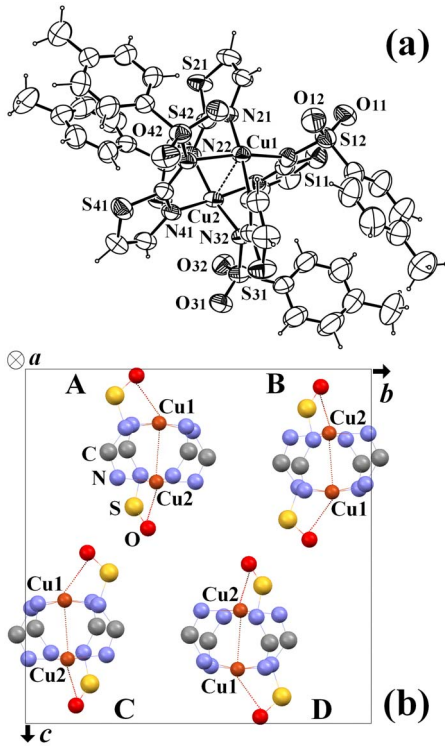
FIG. 1. (Color online) Structure of $Cu_2[TzTs]_4$ (from Ref. 23). (a) ORTEP view of the molecular structure showing the labeling of some of the atoms. (b) Projection along the a axis of the four symmetry related dinuclear units in the unit cell, related by the symmetry operations of the space group $P2_1/c$. The $Cu^1 \cdots Cu^2$ directions of the four units are nearly parallel to the $c*$ axis.

the symmetry operations of the $P2_1/c$ group, sites C and D are connected as sites A and B. An A type unit is connected by these paths to two neighboring B type units [see Fig. 2(b)].

(ii) Cu^1 atoms of neighbor copper dinuclear units A and D at 8.323 Å, related by a C_2 rotation around b followed by an inversion operation, are connected by a bridging network made of two pairs of similar chemical paths labeled as II and III in Figs. 2(a) and 2(b). The equatorial-equatorial paths II

$$CuA^1\text{-}NA\text{-}SA\text{-}CA\text{-}CA - CA - CA - CA - HA \cdots OD - SD$$
$$\text{-}ND\text{-}CuD^1$$

contain 11 diamagnetic atoms including one hydrogen bond connecting a carbon **CA** to an oxygen **OD** with distances **CA-HA** 0.959 Å and **HA···OD** 2.682 Å and an angle **CA-HA···OD** of 144.34° (C-H···O bonds are discussed by Steiner[40]). **NA** and **ND** are equatorially bonded to **CuA**(**CuA-NA**=2.003 Å) and to **CuD**(**CuD-ND** =1.998 Å), respectively. These **Cu**^{1} ions of neighbor dinuclear units A and D (and B and C) are also connected by equatorial-apical paths III,

$$CuA^1\text{-}OA \cdots HD\text{-}CD\text{-}CD\text{-}ND\text{-}CuD^1,$$

containing 5 diamagnetic atoms, including a H bond between an apical oxygen ligand **OA** to **Cu** and a carbon **CD**. The lengths of the corresponding hydrogen bonds are
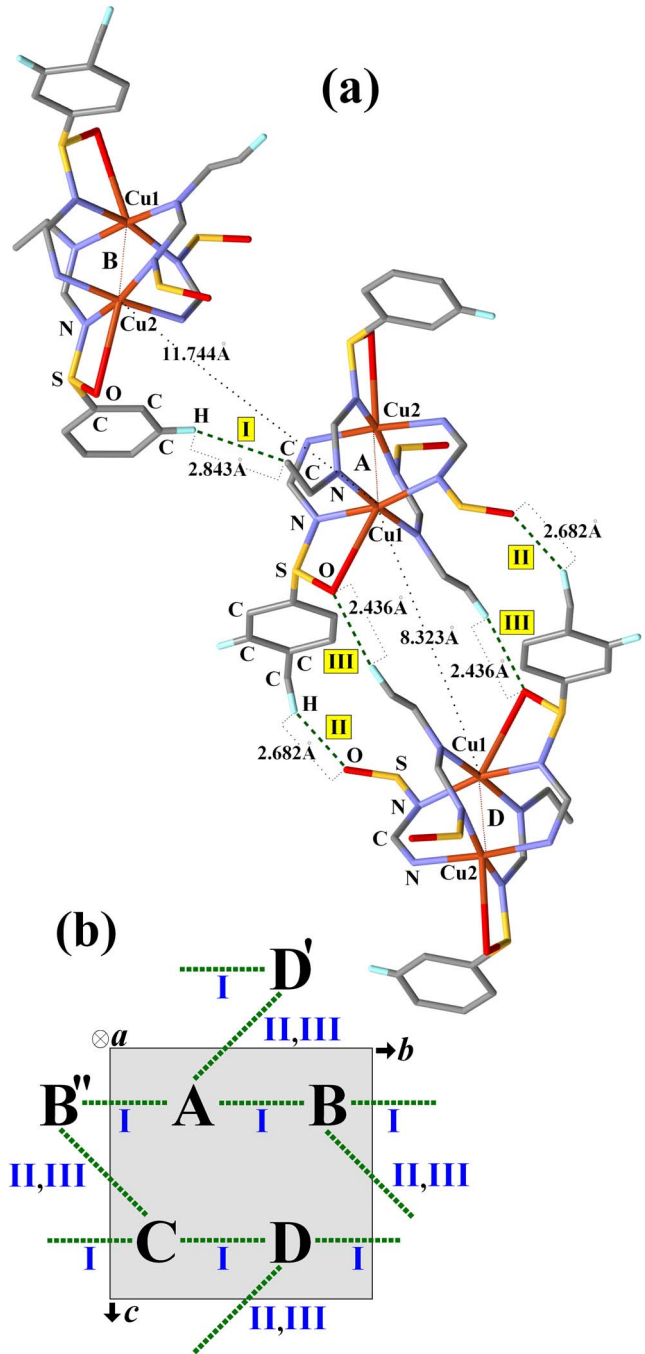

FIG. 2. (Color online) (a) Significant chemical paths connecting dinuclear units in site A with neighbor dinuclear units in sites B and D (see Ref. 23). They are labeled as I, II, and III and all contain hydrogen bonds (see text). (b) Description of the multiplicity of the paths I, II, and III.

OA···HD 2.436 Å and **HD-CD** 0.929 Å and the angle **OA···HD-CD** is 170.03°. This information suggests that the strongest contributions to the superexchange interaction between dinuclear units A and D are through the chemical paths type III, even when this path involves a Cu apical bond. Nevertheless, the four paths act as a whole complex bridging network connecting neighbor dinuclear units type A to units type D [see Fig. 2(b)]. Sites B and C are connected as sites A and D.
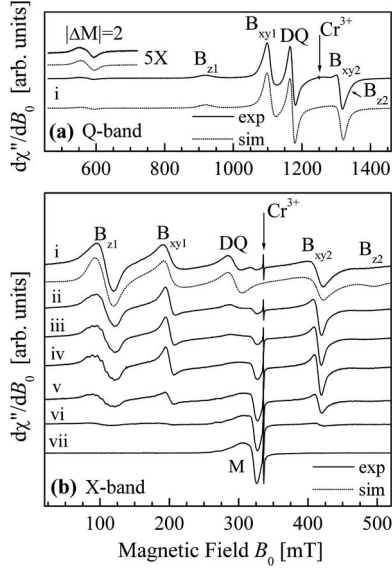
FIG. 3. EPR spectra of a powder sample of $Cu_2[TzTs]_4$. (a) Q band, (b) X band, at several selected temperatures (i=98 K; ii=60 K; iii=50 K; iv=40 K; v=20 K; vi=10 K; vii=4.65 K). The solid lines are experimental results. Dotted lines are spectra simulated using the values in Table I (see text). The double-quantum transition was added at the magnetic field calculated as in Ref. 12. The vertical arrows in (a) and (b) indicate the resonance corresponding to the Cr^{3+}:MgO marker included within the sample.

(iii) The chemical connections between dinuclear units type A and units type C are much weaker than those described above and will not be considered.

A compound with the same chemical formula $Cu_2[TzTs]_4$ was reported by Cejudo-Marín *et al.*[41] who determined its crystal structure. However, different synthetic and recrystallization methods give materials with structures belonging to different space groups and having different lattice parameters. The compound reported by Cejudo-Marín *et al.*[41] is centrosymmetric, with chemically identical copper atoms. The noncentrosymmetric compound studied by Cabaleiro *et al.*,[23] $Cu_2[TzTs]_4$, has a more irregular structure, with an asymmetric unit containing a whole dinuclear molecule.

III. EXPERIMENTAL METHODS

We prepared $Cu_2[TzTs]_4$ and grew single crystals as explained in Ref. 23. Powder samples for EPR measurements were prepared by finely grinding single crystals. Together with the powder samples of $Cu_2[TzTs]_4$ we incorporated small quantities of powdered Cr^{3+}:MgO as field and EPR signal intensity markers (see later). As indicated by x-ray measurements, the single crystals show well-defined (011) growth faces. They were glued to cleaved KCl cubic sample holders conveniently polished to accommodate a (011) growth face so that the a, b, and $c^* = a \times b$ crystal axes are parallel to the x, y, and z axes of the holder, which define the laboratory reference frame (see Fig. 1 of Ref. 42 that describes a similar procedure of single-crystal orientation for an EPR experiment). This procedure allows an accuracy of

$\sim 2°$ in the mounting of good-quality single-crystal samples.

EPR measurements at X band were performed between 4.65 and 110 K with a Bruker ELEXSYS E-580 spectrometer in powder samples and in single-crystal samples at 293 K. EPR measurements at Q band were performed with a Varian E110 spectrometer in a powder sample at 98 and 290 K, and in a single-crystal sample at 293 K.

The integrated intensity of the EPR spectra of finely ground crystalline material measured at X band was evaluated at temperatures (T) between 4.65 and 110 K, by comparison with the integrated intensity of the signal of the Cr^{3+}:MgO marker that has a well-defined paramagnetic behavior of the signal intensity ($1/T$ temperature dependence) in the studied T range.

For the single-crystal experiments, the sample holders described above were positioned on the horizontal plane of a pedestal inside the cavity, and the angular variation of the spectra was measured as a function of magnetic-field orientation $\mathbf{h} = (\sin\theta\cos\phi, \sin\theta\sin\phi, \cos\theta)$, where $\mathbf{B} = B\mathbf{h}$, in the mutually orthogonal crystal planes ab, ac^*, and bc^*. Positions and widths of the resonances were obtained by least-squares fits of field derivative Lorentzian line shapes to the observed spectra. For the analysis of the data and fitting of a spin-Hamiltonian model, we used the program EASYSPIN,[43] working under MATLAB.[44]

IV. EXPERIMENTAL RESULTS

A. Powder samples

Figure 3(a) displays the observed $d\chi''/dB_0$ spectrum of a powder sample of $Cu_2[TzTs]_4$ (solid line) at Q band and 98 K (i) as a function of $B_0 = \mu_0 H$ (μ_0 is the permeability of the vacuum). Above 800 mT it shows the strong peaks labeled B_{xy1}, DQ, and B_{xy2}, and weaker peaks labeled B_{z1} and B_{z2} (shoulder) in the standard notation.[13,14] The peak B_{z2} is under the tail of the B_{xy2} peak, at 1340 mT. The line labeled DQ is a transition between the states $M = \pm 1$ of the spin triplet state, with absorption of two microwave quanta.[13,14] Around 550 mT, the weak one-quantum forbidden transition $\Delta M = \pm 2$ is observed [see amplified inset in Fig. 3(a)].[14] The observed spectra also display the signal of the Cr^{3+} marker (see vertical arrow).

At X band, the powder EPR spectra were measured at 30 temperatures T in the range between 4.65 K and 110 K. Some selected results are displayed in Fig. 3(b). A peak labeled M around $B_0 = 320$ mT ($g \sim 2.1$) is assigned to mononuclear Cu(II) ions present in the sample. The mononuclear species may be due to a small contamination of the powder sample and does not show up in the single crystals. The peaks of the spectrum observed at 98 K [solid line in Fig. 3(b)] are labeled as those at Q band at the same temperature. As discussed later, it is important to note that the hyperfine structure is observed below 50 K in the B_{z1} peak of the dinuclear unit [Fig. 3(b)]. The peak DQ becomes weaker when the temperature is lowered because of a depopulation of the spin triplet. Meanwhile, the M peak increases its intensity with decreasing T, as expected for the paramagnetic behavior of mononuclear Cu. Both results confirm our assignment of the DQ and M peaks. The forbidden transition
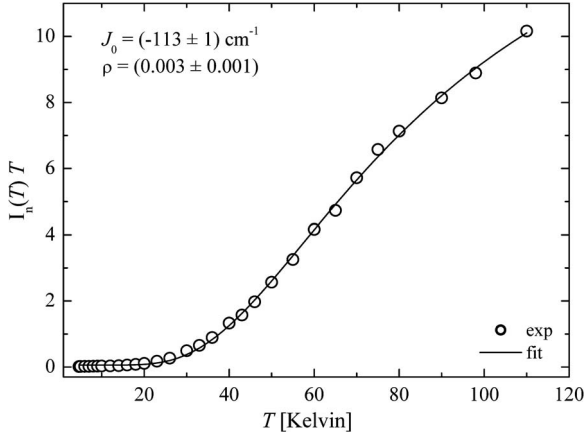
FIG. 4. Temperature variation of the ratio between the integrated intensities of the spectra at X band of a powder sample of $Cu_2[TzTs]_4$ and for the marker (see Fig. 3), multiplied by the temperature. The dotted line is the best fit with the Bleaney and Bowers equation [Eq. (1)].

$\Delta M = \pm 2$ is superposed with B_{z1} and, at X band, the B_{z2} line appears at 485 mT. At X band and each T we calculated a normalized intensity ratio I_n between the integrated intensity of the powder spectra and that of the signal corresponding to the $MgO:Cr^{3+}$ marker [indicated by a vertical arrow in Fig. 3(b)], and the result is displayed as $I_n \times T$ vs T in Fig. 4. This value decreases with decreasing temperature, as expected for antiferromagnetically coupled dinuclear units with an EPR-silent ground singlet state and an excited triplet state.[10] This procedure avoids considering possible changes of the experimental setup when changing T, allowing accurate evaluation of the temperature variation of the population of the excited triplet $S=1$ state of the dinuclear units and thus the splitting between singlet and triplet states of the dinuclear unit, that equals the exchange interaction J_0. To do that we used the Bleaney and Bowers[16] equation for the magnetic susceptibility, as modified by Kahn,[17] to consider the presence of small quantities of mononuclear paramagnetic centers,

$$\chi(T) \times T = \frac{2N_{Av}g^2\mu_B^2}{k_B} \left\{ \frac{1-\rho}{[3+\exp(-J_0/k_BT)]} + \frac{1}{4}\rho \right\}, \quad (1)$$

where ρ is the molar fraction of noncoupled species, k_B is the Boltzmann constant, T is the temperature, μ_B is the Bohr magneton, and N_{Av} is the Avogadro number. Since the values of $I_n \times T$ in Fig. 4 are not absolute quantities but proportional to $\chi(T) \times T$, only the temperature dependence is relevant, and the g value appearing in Eq. (1) cannot be obtained from this fitting. A least-squares fit of Eq. (1) to the data in Fig. 4 gives $J_0 = (-113 \pm 1)$ cm^{-1} and $\rho = 0.003 \pm 0.001$. The ratio ρ between the numbers of mononuclear and dinuclear units is small, and its relative uncertainty is large. However, the amplitude of the EPR signal corresponding to mononuclear Cu units is similar to that of dinuclear units because the field spread of the mononuclear Cu(II) signal is about 10 times smaller than that of the spectrum for the dinuclear unit. Correspondingly, this weak peak is amplified ~2 orders of magnitude in comparison with the others.
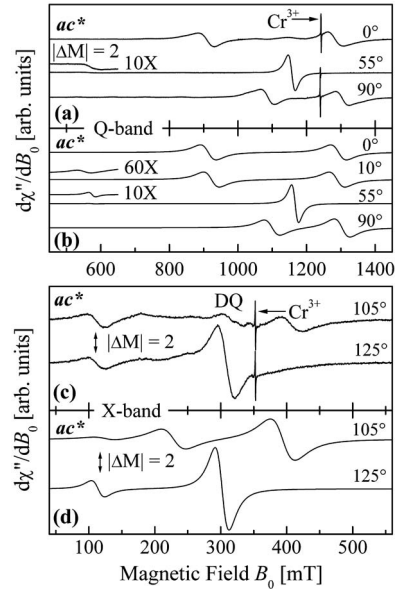

FIG. 5. Single-crystal EPR spectra observed at Q band (a) and X band (c), for specific orientations of the magnetic field in the $ac*$ plane at room temperature. The angles are given in the laboratory coordinate system $abc* \equiv xyz$ described in the text. Spectra simulated using EASYSPIN at the same angles are displayed in (b) and (d); they show that the forbidden transition disappears at 0° and 90°. At 10° this transition is very weak and not observed. Note that at X band the DQ transition appears at the same magnetic-field region where the collapse occurs.

B. Single-crystal samples

Typical spectra of single-crystal samples of $Cu_2[TzTs]_4$ observed at Q and X bands in the plane ac^* at room temperature are displayed in Figs. 5(a) and 5(c), respectively. Similar results are obtained in the bc^* plane (not shown). At Q band three resonance lines are observed for most orientations of B_0 in the ac^* and bc^* planes. Two are strong and anisotropic and correspond to the "allowed" $M = \pm 1 \leftrightarrow 0$ transitions, within the $S=1$ triplet of the dinuclear unit. The third resonance shown for $\theta = 55°$ in the insets of Figs. 5(a) and 5(b) amplified 10 times is weak and corresponds to the "forbidden" $M = \pm 1 \leftrightarrow \mp 1$ transition.[14] In the ab plane the positions of the allowed transitions do not change with angle. The forbidden transition is not observed in the plane ab, or close to the a and b axes in the planes ac^* and bc^*, as it would be expected for a zero-field splitting with uniaxial symmetry around the $z=c^*$ axis. No hyperfine splitting is resolved at any orientation of the field in the single-crystal spectra.

Careful fittings of functions containing one and two Lorentzian first derivative functions to the observed signals were performed in order to calculate their positions and widths. The angular variations of the positions at Q and X bands, observed at 293 K, in the planes ac^*, bc^*, and ab are displayed in Figs. 6(a)–6(c) and 7(a)–7(c). The maximum splittings between the allowed transitions [up and down triangles in Figs. 6(a), 6(b), 7(a), and 7(b)] occur for the magnetic-field along the c^* axis of the dinuclear units ($\theta = 0°$). It is noteworthy that we observe the spectrum of only
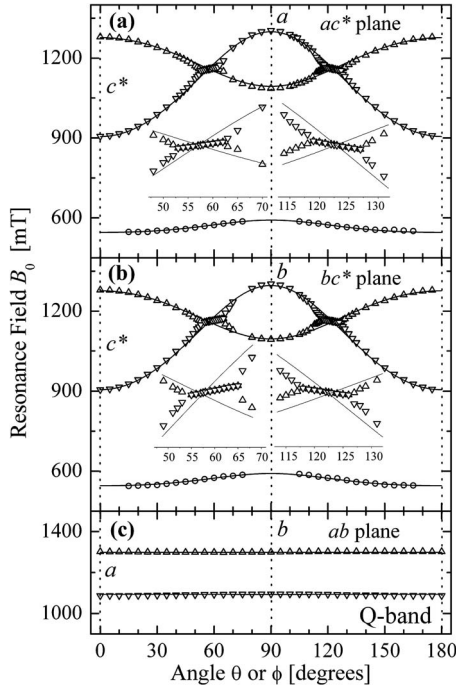
FIG. 6. Positions of the resonances observed at 34.5 GHz and $T = 293$ K with the magnetic field in the three planes: (a) ac^*, (b) bc^*, and (c) ab planes. Triangles indicate the $M = \pm 1 \rightarrow 0$ transitions. The maximum splitting between them is along the c^* axis. They collapse at the magic angles ($54.7°$ and $125.3°$ from the c^* axis) in the ac^* and bc^* planes. The circles indicate the "forbidden" resonance with $|\Delta M| = 2$ that is observed only in the ac^* and bc^* planes, far from the axes. The solid lines were obtained using the parameters of Table I calculated with the EASYSPIN program (Ref. 43). The insets in (a) and (b) show with higher detail the regions where the resonances collapse for orientations of the field around the magic angles in the ac^* and the bc^* planes. There is not a single crossing of the signals at the magic angles, but a collapse occurs in wide angular ranges.

one type of dinuclear unit. This indicates that the peaks corresponding to the A and B units related by a C_2 symmetry operation [see Figs. 1(b) and 2(a)] are too close and they are collapsed by the exchange interactions connecting them.[28]

Near the magic angles $\theta_m = 54.7°$ and $125.3°$ with the c^* $= z$ axis in the ac^* and bc^* planes [see Figs. 6(a), 6(b), 7(a), and 7(b)], the allowed resonances collapse, as expected for a dipolar interaction. The collapse is defined when the quality factor of the fitting with two signals equals that obtained with one signal. However, the collapses are not simple intersections of the curves indicating the line positions, but occur within an unexpectedly wide angular range around θ_m [see the insets showing the line positions near the two magic angles in each plane in Figs. 6(a) and 6(b)]. Similar collapses occur at X band [Figs. 7(a) and 7(b)], but the accuracy of these measurements are poorer because the collapsing transitions are superimposed to the double-quantum transition. The line widths of the main EPR peaks observed at Q band in the ac^* and bc^* planes are shown in Figs. 8(a) and 8(b) as a function of magnetic-field orientation. Both peaks have the same nearly isotropic width except in the angular region
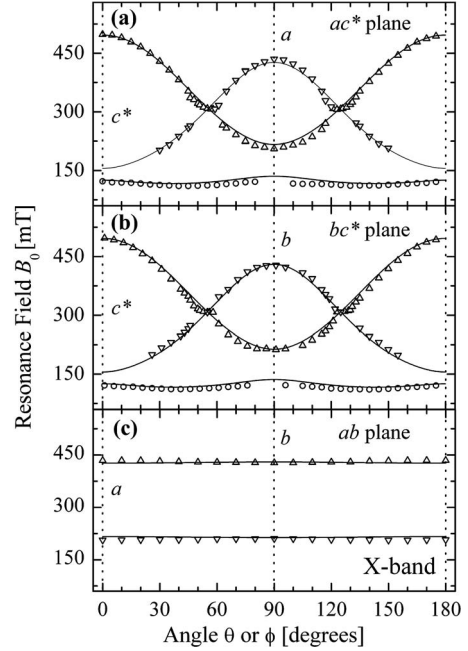

FIG. 7. Position of the resonances observed at 9.5 GHz and $T = 293$ K with the magnetic field in the three studied planes: (a) ac^*, (b) bc^*, and (c) ab planes. Triangles indicate $M = \pm 1 \rightarrow 0$ transitions. The maximum splitting between them is along the symmetry axis c^*. They collapse at the magic angles ($54.7°$ and $125.3°$) in the ac^* and bc^* planes. The collapse occurs as observed as Q band occurs, but the quality of the data is poorer because of the overlapping of the signals with the DQ signal. The circles indicate the forbidden resonance with $|\Delta M| = 2$, that is observed only in the ac^* and bc^* planes, far from the axes. The solid lines were obtained with the parameters given in Table I.

where they are collapsed and the width of the single line is strongly reduced.

In Figs. 9(a)–9(d) we display plots suggested by the theory of Anderson and Weiss[3,4] for the positions of the resonances around the magic angles in the ac^* and bc^* planes,
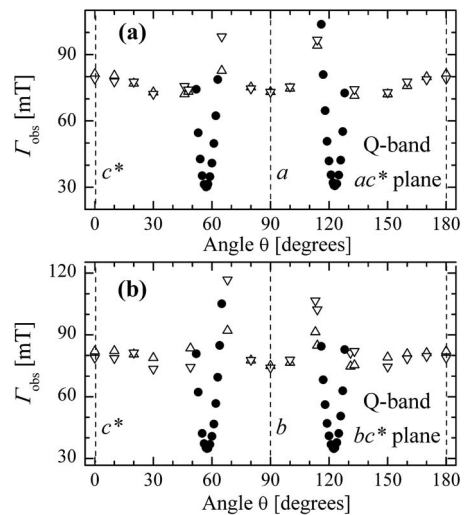

FIG. 8. (a) Width of the $\pm 1 \rightarrow 0$ signal in the ac^* plane and (b) in the bc^* plane. A strong reduction of the width occurs around the magic angles where the signals collapse.
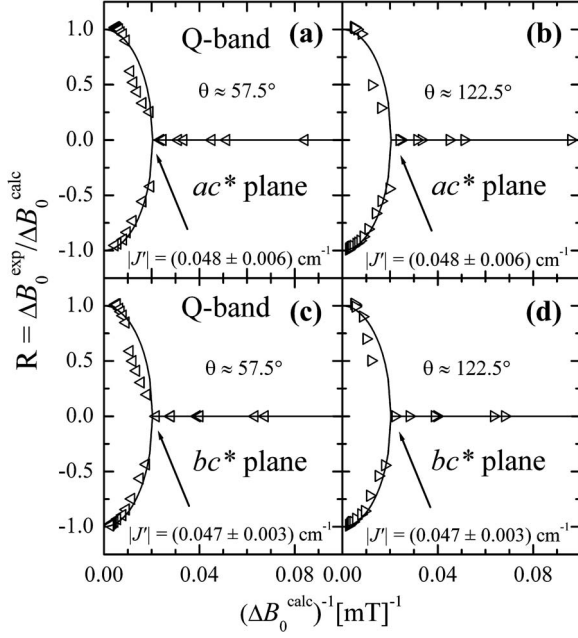
FIG. 9. Plot of the rate $R = \Delta B_0^{\mathrm{exp}}/\Delta B_0^{\mathrm{calc}}$ as a function of $(\Delta B_0^{\mathrm{calc}})^{-1}$. $\Delta B_0^{\mathrm{exp}}$ and $\Delta B_0^{\mathrm{calc}}$ are the observed and calculated separations of the signals around the two magic angles in the ac^* and bc^* planes (Anderson's plot). (a) and (b) correspond to the ac^* plane; (c) and (d) correspond to the bc^* plane.

respectively. The ratio between the observed and the calculated splittings of the two lines near and within the collapsed angular range is plotted versus the calculated separation of these two lines. The exchange coupling between neighbor dinuclear units will be calculated from these results (see later).

Figures 10(a)–10(d) display the line width of the collapsed resonance observed in the ac^* and bc^* planes in the narrow angular regions around the magic angles where the signals collapse, and the line width displays a strong decrease with a parabolic angular dependence around the magic angle. This parabolic angular dependence is discussed later and used to evaluate the exchange couplings between neighbor dinuclear units in a different way. As discussed in the theoretical section, in these angular ranges the width varies quadratically with the splitting of the lines expected in the absence of collapse.

V. MAGNETIC INTERACTIONS AND ELECTRON-PARAMAGNETIC RESONANCE SPECTRA

The spin-Hamiltonian operators describing the EPR spectra of dinuclear units weakly coupled by interdinuclear exchange interactions like in $Cu_2[TzTs]_4$ can be written as:

$$\mathcal{H} = \mathcal{H}_0 + \mathcal{H}_1 = \sum_i (\mathcal{H}_{\mathrm{ex}}^i + \mathcal{H}_{\mathrm{anis}}^i + \mathcal{H}_z^i) + \mathcal{H}_1, \quad (2)$$

where the sum is over the units i. In Eq. (2), $\mathcal{H}_{\mathrm{ex}}^i$ is the isotropic (Heisenberg) exchange interaction within the unit i,

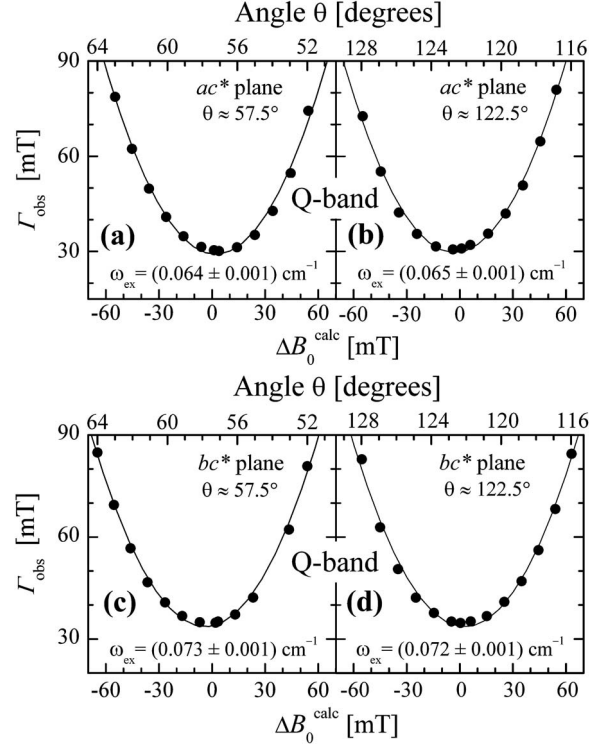$$\mathcal{H}_{\mathrm{ex}}^i = -J_0 \mathbf{S}_{1,i} \cdot \mathbf{S}_{2,i}. \quad (3)$$

Meanwhile,

FIG. 10. [(a) and (b)] Width of the $\pm 1 \to 0$ signal in the ac^* plane and [(c) and (d)] in the bc^* plane. A strong reduction of the width occurs around the magic angles where the signals collapse. The solid lines (parabolas) in the collapsed regions around the magic angles are calculated by fitting Eq. (18) to the experimental results. The corresponding values of ω_{ex} are included in Table II.

$$\mathcal{H}_{\mathrm{anis}}^i = \mathbf{S}_{1,i} \cdot \mathcal{D} \cdot \mathbf{S}_{2,i} \quad (4)$$

contains anisotropic spin-spin interactions between Cu(II) ion pairs in a dinuclear unit (mainly dipole-dipole interactions, but also symmetric anisotropic exchange).[14] $\mathcal{H}_z^i$ is the Zeeman interaction coupling the spins in the i unit with the external magnetic field $\mathbf{B}_0$,

$$\mathcal{H}_z^i = \mu_B \mathbf{B}_0 \cdot (\mathbf{g}_1 \cdot \mathbf{S}_{1,i} + \mathbf{g}_2 \cdot \mathbf{S}_{2,i}), \quad (5)$$

where the $\mathbf{g}$ matrices (see Ref. 45) $\mathbf{g}_1$ and $\mathbf{g}_2$ in Eq. (5) correspond to Cu sites 1 and 2. The fact that $Cu_2[TzTs]_4$ contains anisotropic Cu(II) ions and Cu(II) dinuclear units with rotated orientations in the unit cell (and thus rotated g matrices) imposes special problems[28] that are discussed later. Finally,

$$\mathcal{H}_1 = -\sum_{i,j \neq i} [J_1(i,j)\mathbf{S}_{1,i} \cdot \mathbf{S}_{1,j} + J_3(i,j)\mathbf{S}_{2,i} \cdot \mathbf{S}_{1j}$$
$$+ J_2(i,j)\mathbf{S}_{1,j} \cdot \mathbf{S}_{2,j} + J_4(i,j)\mathbf{S}_{2,i} \cdot \mathbf{S}_{2,j}], \quad (6)$$

where the $\mathbf{S}_{p,i}$ are the spin 1/2 operators corresponding to a copper type p ($p = 1, 2$) in the ith dinuclear unit. Equation (6) contains the isotropic exchange couplings between copper ions in different units which are associated to specific interdinuclear exchange paths (see crystallographic description), involving interactions with a distribution of magnitudes. Anisotropic spin-spin interactions between copper ions in

neighbor dinuclear units are smaller and are neglected for our purpose (see later).

General theories of magnetic resonance[4–8] relate the Fourier transform of the EPR line shape $I(\omega)$ to the thermal averages of the time-correlation function of the magnetization along the microwave magnetic-field direction:

$$I(\omega) = \frac{1}{2\pi} \int_{-\infty}^{\infty} G(t) e^{-i\omega t} dt, \tag{7}$$

where

$$G(t) = \int_{-\infty}^{\infty} I(\omega) e^{i\omega t} d\omega = \frac{\langle M_x(t) M_x(0) \rangle}{\langle M_x(0) M_x(0) \rangle}$$

$$= \frac{\mathrm{tr}[e^{-\mathcal{H}/k_B T} M_x(t) M_x(0)]}{\mathrm{tr}[e^{-\mathcal{H}/k_B T} M_x^2(0)]}, \tag{8}$$

where $M_x(t)$ is the magnetization operator in the Heisenberg representation:

$$M_x(t) = e^{i\mathcal{H}t/\hbar} M_x e^{-i\mathcal{H}t/\hbar}. \tag{9}$$

The time dependence of $M_x(t)$ is induced by the perturbation $\mathcal{H}_1$ that contains the stochastic interactions of the system with the environment. The averages $\langle \cdots \rangle$ in Eq. (8) are over the states of this environment. The experiment performed at room temperature can be analyzed using the high-temperature approximation, $e^{-\mathcal{H}/k_B T} \approx \mathbf{I}$, where $\mathbf{I}$ is the unit matrix.[8] At lower T this is not valid (see later). A simple solution given by Kubo[6,7] for the time variation of M_x arising from Eq. (9) when the values of Ω are shifted to give a mean value $\langle \Omega(t) \rangle = 0$ is:

$$\frac{dM_x(t)}{dt} = i\Omega(t) M_x(t). \tag{10}$$

The random function $\Omega(t)$ in Eq. (10) is characterized by an amplitude, given by its second moment Δ, and a coherence time given by an exchange-correlation time τ_{ex}, or (equivalently) an "exchange frequency" ω_{ex} where

$$\Delta = \langle \Omega^2 \rangle^{1/2} \quad \text{and} \quad \tau_{\mathrm{ex}} = \frac{2\pi}{\omega_{\mathrm{ex}}} = \int_0^{\infty} \frac{\langle \Omega(t)\Omega(0) \rangle}{\Delta^2} dt. \tag{11}$$

When the product $\Delta \tau_{\mathrm{ex}} \gg 1$, the modulation of Ω is said to be slow; if $\Delta \tau_{\mathrm{ex}} \ll 1$ the modulation is fast.[4–7] In our experiments we moved between these two conditions. In our problem Ω is the frequency associated to the anisotropic or dipolar coupling within a dinuclear unit and τ_{ex} (or ω_{ex}) is associated to the effect of the exchange interactions included in $\mathcal{H}_1$. When the interaction $\mathcal{H}_1$ in Eq. (6) is negligible, the Hamiltonian $\mathcal{H}$ of Eq. (2) breaks up into independent contributions for each unit i; there is no environment and the problem is solved by well-known methods.[11–14] When $\mathcal{H}_1$ is relevant, the complex many-body problem is not separable but can be solved by approximate methods using stochastic techniques[3–7] (see also Abragam[8] and Pake[9]). Applications of these theories to calculate exchange couplings from the EPR spectra of a continuum set of weakly interacting anisotropic spins 1/2 (instead of dinuclear units) have been recently reviewed by Calvo.[28] To accomplish the analysis of coupled

dinuclear units, we proceed by steps of increasing complexity, considering first the zeroth-order contribution $\mathcal{H}_0$ to Eq. (2), and later, $\mathcal{H}_1$ that couples these units.

A. Spin-Hamiltonian and electron-paramagnetic resonance spectra of isolated dinuclear units

We rationalize first the spectra observed for noninteracting dinuclear units described by $\mathcal{H}_0$ of Eq. (2).[11–14] $\mathcal{H}_0$ does not include hyperfine couplings that at high T are averaged out by the exchange couplings between dinuclear units and contribute only to the line width (see later). It also neglects antisymmetric exchange contributions,[12] assuming that the dinuclear units under study have an inversion center (as closely occurs for $Cu_2[TzTs]_4$).

A convenient transformation of the spin operators is

$$\mathbf{S} = \mathbf{S}_1 + \mathbf{S}_2, \quad \mathbf{s} = \mathbf{S}_1 - \mathbf{S}_2 \quad \text{or equivalently } \mathbf{S}_1 = 1/2(\mathbf{S} + \mathbf{s}),$$

$$\mathbf{S}_2 = 1/2(\mathbf{S} - \mathbf{s}), \tag{12}$$

where $\mathbf{s}$ does not follow spin-operator commutation rules. Equations (12) allow writing

$$\mathcal{H}_0 = \mu_B \mathbf{B} \cdot [\mathbf{g} \cdot \mathbf{S} + \mathbf{G} \cdot \mathbf{s}] - 1/2 J_0 S(S+1)$$

$$+ 1/4[\mathbf{S} \cdot \mathcal{D} \cdot \mathbf{S} - \mathbf{s} \cdot \mathcal{D} \cdot \mathbf{s}], \tag{13}$$

where we discard the sum over similar units in $\mathcal{H}_0$, considering a single dinuclear unit, and neglect constants shifting equally all levels. Since $S_1 = S_2 = 1/2$, $S = 1$ or 0, in Eq. (13), $\mathbf{g} = (\mathbf{g}_1 + \mathbf{g}_2)/2$ and $\mathbf{G} = (\mathbf{g}_1 - \mathbf{g}_2)/2$ and one can define a zero-field splitting matrix (see Ref. 45) $\mathbf{D} = \mathcal{D}/4$ to describe the spectrum arising from the $S = 1$ triplet, in terms of the intradinuclear anisotropic interactions. For dinuclear units of spins 1/2, the contribution $\mathbf{s} \cdot \mathbf{D} \cdot \mathbf{s}$ has matrix elements between the states with $S = 0$ and $S = 1$ (having an energy splitting J_0), but not within the $S = 1$ triplet.[14] Since the EPR spectra arise from transitions within the $S = 1$ triplet, the contribution of $\mathbf{s} \cdot \mathbf{D} \cdot \mathbf{s}$ can be neglected when $|J_0| \gg |\mathbf{D}|$. Thus, Eq. (13) is written as:

$$\mathcal{H}_0 = \mu_B \mathbf{B_0} \cdot [\mathbf{g} \cdot \mathbf{S} + \mathbf{G} \cdot \mathbf{s}] - 1/2 J_0 S(S+1) + \mathbf{S} \cdot \mathbf{D} \cdot \mathbf{S}. \tag{14}$$

The powder and single-crystal spectra predicted by Eq. (14) can be calculated in terms of 12 parameters arising from $\mathbf{g}_1$ and $\mathbf{g}_2$ (or, alternatively, from $\mathbf{g}$ and $\mathbf{G}$), plus five parameters arising from the traceless symmetric $\mathbf{D}$ matrix (D, E, plus 3 Euler angles) which may be referred to the laboratory system of axes $xyz \equiv abc^*$. Thus, neglecting J_0 that contributes only to the temperature dependence of the signal amplitude of the spin triplet, exact calculation of the spectrum of the dinuclear unit involves 17 spin-Hamiltonian parameters, plus those related to line broadening. Evaluating these parameters from the data would be difficult because they are strongly correlated, requiring well isolated dinuclear units and single-crystal measurements with narrow resonances. Simplifications of the spin Hamiltonian have to be made in most cases. The simplest is to neglect the "residual Zeeman contribution" $\mathcal{H}_z' = \mu_B \mathbf{B}_0 \cdot \mathbf{G} \cdot \mathbf{s}$ (six parameters), possible

TABLE I. Spin-Hamiltonian parameters obtained from the EPR results at Q and X bands using EASYSPIN[43] in powder and single-crystal samples. Averages are over single-crystal results at both microwave frequencies.

EPR parameters	Powder samples		Single-crystal samples		Averages
Frequency [GHz]	34.616	9.308	33.334	9.7844	
g_{xx}	2.032	2.031	2.043	2.063	2.042 ± 0.011
g_{yy}	2.041	2.042	2.044	2.063	2.047 ± 0.008
g_{zz}	2.224	2.208	2.249	2.248	2.232 ± 0.016
D [cm^{-1}]	0.201	0.201	0.195	0.195	(0.198 ± 0.003) cm^{-1}
E [cm^{-1}]	0.0017	0.0016	0.0012	0.0010	(0.001 ± 0.003) cm^{-1}

1 cm^{-1} = $1.98644746 \times 10^{-23}$ Joule = $2.99792458 \times 10^{+4}$ MHz.

when $\mathbf{g}_1$ and $\mathbf{g}_2$ are not too different, as for units close to having inversion symmetry. It is also possible because $\mathcal{H}_z'$ does not commute with the exchange coupling $-J_0 \mathbf{S}_1 \cdot \mathbf{S}_2$ and it is asymptotically reduced to zero as $|\mathcal{H}_z'|^2/|J_0|$ (see text and Fig. 1 of Ref. 28 for further details). Thus, we have kept only the main Zeeman term $\mu_B \, \mathbf{B}_0 \cdot \mathbf{g} \cdot \mathbf{S}$, eliminating six parameters in the simulation. One may also consider that the matrices $\mathbf{g}$ and $\mathbf{D}$ (see Ref. 45) have the same principal axes (thus eliminating three Euler angles). In summary, the spectrum of a dinuclear unit is similar to that expected for a spin $S=1$, showing two anisotropic allowed transitions $M=\pm 1 \leftrightarrow M=0$ around $g \sim 2$, one forbidden transition $M=+1 \leftrightarrow M=-1$ at a field corresponding to $g \sim 4$ and a double-quantum transition $M=+1 \leftrightarrow M=-1$ at $g \sim 2$, involving two photons.[11–14]

Figure 1(b) shows the four dinuclear units in the unit cell related by the symmetry operations of the space group $P2_1/c$ (see structural section). They should give rise to two spectra corresponding to units A and C and to units B and D (the inversion operation relating units A with C and B with D makes equal the spectra of these pairs). In a single crystal with narrow signals and in the absence of coupling between the units, one should see two pairs of central resonances (corresponding to the allowed transitions of two dinuclear units) with angular variation of positions differing by a C_2 rotation around b. However, as shown in Figs. 5–7, only one pair of allowed transitions from the dinuclear units are observed. In fact the unit cell of Cu$_2$[TzTs]$_4$ displayed in Fig. 1(b) shows that the directions Cu^1-Cu^2 are nearly parallel to the c^* axis (the angle between those corresponding to units A and B is only $\sim 5°$). Thus, exchange couplings between neighbor dinuclear units average out the small spectral differences of rotated units[28] explaining the collapse of their resonances. In that case the spectra are described by five independent spin-Hamiltonian parameters. We simulated the single-crystal spectra as a function of angle (Fig. 5) and the angular variation of the line positions (Figs. 6 and 7) using EASYSPIN.[43] With an optimization program we calculated the five parameters (three principal values of the $\mathbf{g}$ matrix and two principal values of the $\mathbf{D}$ matrix) from the observed angular variation, neglecting the points close to the magic angles where the resonances collapse. The parameters obtained at Q and X bands are given in Table I. Figures 5(b) and 5(d) display spectral simulations obtained with the parameters of Table I for the single-crystal samples at the same

angles as in Figs. 5(a) and 5(c). EASYSPIN does not reproduce the double-quantum transition[46] that was added to the simulation as explained in Ref. 12. Obviously, the additional peak corresponding to mononuclear Cu ions is not reproduced. The simulations also show that the forbidden transition vanish at $\theta=0°$ (c^* axis) and at $\theta=90°$ (a axis) where the transition probabilities are zero, as observed experimentally. For B_0 close to the axes [e.g., $\theta=10°$ with the c^* axis in Fig. 5(b)], these intensities are very small.

The calculated angular variation of the positions of the peaks are given as solid lines in Figs. 6 and 7 and reproduce well the experimental result except for field orientations close to the magic angles in the planes ac^* and bc^* where, as expected, the calculated angular dependence shows a simple crossing and not the observed collapsed angular range [see insets in Figs. 6(a) and 6(b)]. We also simulated the powder spectra at Q and X bands at 98 K and using an optimization program calculated the parameters included in Table I, which were used to obtain the dotted lines in Figs. 3(a) and 3(b). A surprising result is that the rhombic zero-field splitting parameter E calculated from single crystal and powder data is zero within the accuracy of the experiment for dinuclear units whose structure do not have axial symmetry. This result confirms that the observed spectra are the average of the spectra corresponding to the two rotated dinuclear units in the unit cell[28] that should have axial symmetry around the $z=c^*$ axis.

B. The random coupling approach to the quantum phase transition

We treat the exchange interactions included in $\mathcal{H}_1$ transforming Eq. (6) to a base of product functions of the singlet s and triplet t states (for $S=0,1$) of units (i) and (j):

$$t(i) \otimes t(j), \quad s(i) \oplus t(j), \quad t(i) \otimes s(j), \quad s(i) \oplus s(j).$$

Since we observe the triplet state, only matrix elements of Eq. (6) connecting the nine states of the subspace $t(i) \otimes t(j)$ are relevant. Projecting Eq. (6) over this subspace we obtain:

$$\mathcal{H}_1 = -\frac{1}{4} \sum_{i,j \neq i} [J_1(i,j) + J_2(i,j) + J_3(i,j) + J_4(i,j)] \mathbf{S}_{(i)} \cdot \mathbf{S}_{(j)},$$

$$(15)$$

where $\mathbf{S}_{(i)}$ and $\mathbf{S}_{(j)}$ are spin one operators corresponding to the dinuclear units (i) and (j). The factor 1/4 is a result of the

TABLE II. Values of the exchange frequencies calculated from (a) Anderson's plots displayed in Figs. 9(a)–9(d) and (b) from the angular variation of the line width around the magic angles [Figs. 8(a), 8(b), and 10(a)–10(d)].

Angle/plane	$57.5°/ac^*$ plane	$122.5°/ac^*$ plane	$57.5°/bc^*$ plane	$122.5°/bc^*$ plane
(a) From collapse	$\hbar\omega_{ex}=(0.048\pm0.006)$ cm^{-1}	$\hbar\omega_{ex}=(0.048\pm0.006)$ cm^{-1}	$\hbar\omega_{ex}=(0.047\pm0.003)$ cm^{-1}	$\hbar\omega_{ex}=(0.047\pm0.003)$ cm^{-1}
(b) From line width	$\hbar\omega_{ex}=(0.064\pm0.005)$ cm^{-1}	$\hbar\omega_{ex}=(0.065\pm0.006)$ cm^{-1}	$\hbar\omega_{ex}=(0.073\pm0.006)$ cm^{-1}	$\hbar\omega_{ex}=(0.072\pm0.005)$ cm^{-1}
	$\Gamma_0=(29.2\pm0.7)$ mT	$\Gamma_0=(29.7\pm0.6)$ mT	$\Gamma_0=(33.8\pm0.5)$ mT	$\Gamma_0=(33.7\pm0.7)$ mT

1 cm$^{-1}=1.98644746\times10^{-23}$ Joule$=2.99792458\times10^{+4}$ MHz.

transformation to the triplet states. When a unit (i) is taken as the center of the problem, there is a distribution of parameters $J_\alpha(i,j)$ ($\alpha=1,...,4$) corresponding to all neighboring dinuclear units. The infinite terms contributing to $\mathcal{H}_1$ in Eq. (15) behave as a "random environment" of exchange-coupled units j observed by each single individual unit i. We attribute to this random interaction the experimental results shown in the insets of Fig. 6 and in Figs. 9 and 10 and treat the problem with the Anderson model[3,4] of exchange narrowing of magnetic-resonance lines, which provides the simplest physical arguments and the methodology to estimate mean values of the interactions from the data. Anderson's model requires some basic conditions:

(a) As described by Van Vleck[2] for the dipolar interaction, the anisotropic contribution $\mathcal{H}_{anis}$ to Eq. (2) is assumed to be diagonal so it has no matrix elements connecting different states. This is the adiabatic approximation, important for the simplicity of the treatment. It is approximate valid for the dipolar interaction in the presence of a sufficiently large magnetic field.[8]

(b) $\mathcal{H}_1$ commutes with the total magnetic-moment operator M appearing in the line-shape expression [Eq. (8)]:

$$\mathbf{M}=-\mu_B\sum_i(\mathbf{g}_1\cdot\mathbf{S}_{1,i}+\mathbf{g}_2\cdot\mathbf{S}_{2,i}). \quad (16)$$

This is exactly valid when $\mathbf{g}_1=\mathbf{g}_2$ (for dinuclear units having inversion symmetry). However, this problem has been treated elsewhere[28,47,48] and does not introduce a limitation to our present objective.

(c) $\mathcal{H}_1$ also commutes with the Zeeman interaction $\mathcal{H}_Z=-\mathbf{M}\cdot\mathbf{B}_0$ [Eq. (5)], a condition that holds in the same case indicated for (**b**).

(d) $\mathcal{H}_1$ does not commute with $\mathcal{H}_{anis}$, which is time modulated and thus reduced or averaged out by $\mathcal{H}_1$.

In our experiments we observe a dipolar line structure of the resonances of isolated dinuclear units, and not the dipolar broadening observed in the classical studies. We follow the collapse of this fine structure introduced by $\mathcal{H}_{anis}$ produced by the random distribution of interactions included in $\mathcal{H}_1$ [Eq. (15)]. This provides a more direct and physically appealing observation of the exchange-narrowing phenomena for the dipolar interaction than obtained before.[8,9] As described recently by Pastawski,[32] the problem confronted here is a case of a much general problem occurring with the oscillatory dynamics of a quantum system which, in the presence of an infinite random environment, undergo a quantum dynamical phase transition to a nonoscillatory phase. We treat first the results in Figs. 9(a)–9(d) where the fine struc-

ture introduced by the (mainly) dipolar interaction within the dinuclear units collapses as a consequence of the interaction with neighboring dinuclear units. Later we treat the characteristic angular variation of the line width observed around the magic angles and displayed in Figs. 10(a)–10(d). These widths of the resonances around the magic angles in the ac^* and bc^* planes provide complementary sources of information about the exchange interactions between dinuclear units.

1. Analysis of the collapse of the resonances

The symbols in Figs. 9(a)–9(d) display the ratio $R=\Delta B_0^{exp}/\Delta B_0^{calc}$ between the observed distances between the collapsing resonances and the average position, as a function of the reciprocal of the calculated distance, for the magnetic-field oriented near the two magic angles in the planes ac^* and bc^*. This type of graph was proposed by Anderson[4] and offers a normalized view of the collapse of the signals. It was used later by Martino *et al.*[26,27] (see also Ref. 28) to study the collapse of EPR signals arising from mononuclear species in rotated lattice sites. When ΔB_0^{calc} is small ($1/\Delta B_0^{calc}$ large), close to the magic angles, the signals are collapsed and $R=0$. When ΔB_0^{calc} is large, far from the magic angles, $R\sim\pm1$. The collapse occurs when $g\mu_B[\Delta B_0^{calc}]_{collapse}=\hbar\omega_{ex}$ [$\omega_{ex}=2\pi/\tau_{ex}$ is defined by Eq. (11)], a condition allowing to obtain the exchange frequency ω_{ex} from the well defined collapse of the signals in Figs. 9(a)–9(d). The results for the exchange frequency ω_{ex} given in Table II were also obtained by fitting the function[3,4,26–28]

$$R=\frac{\Delta B_0^{exp}}{\Delta B_0^{calc}}=\pm\sqrt{1-\left(\frac{\hbar\omega_{ex}}{g\mu_B\Delta_0^{calc}}\right)^2} \quad (17)$$

to the data in Figs. 9(a)–9(d) in the noncollapsed region with very similar results. The solid lines in these figures are obtained from these fittings.

2. Analysis of the line width

Anderson's theory indicates that the observed line width of the resonance in the collapsed region, Γ_{obs} (in mT), is given by:

$$\Gamma_{obs}=\frac{g\mu_B(\Delta B_0^{calc})^2}{\hbar\omega_{ex}}+\Gamma_0, \quad (18)$$

where ΔB_0^{calc} is the field distance between the collapsing lines which would be observed in the absence of exchange extracted from the information plotted as solid lines in Fig. 6. Since near the magic angles ΔB_0^{calc} varies linearly with

angle, the width of the collapsed resonance Γ_{obs} should vary quadratically with the distance to the magic angles, as observed experimentally [see Figs. 10(a)–10(d)]. Γ_0 is a contribution to the width arising from other broadening sources; in the narrow collapsed angular range of Fig. 10 it may be considered a constant (see Fig. 8). Equation (18) allows us to calculate from these experimental results the values of ω_{ex} and Γ_0 included in Table II and provides the solid lines in Figs. 10(a)–10(d).

3. Interdinuclear exchange interactions

The values of $\hbar\omega_{ex}$ obtained from the data and given in Table II are related to the exchange couplings between neighbor dinuclear units [Eq. (6) or (15) in the spin 1 representation). This relationship has been described by Levstein and Calvo,[47] Brondino *et al.*,[49] and Passeggi and Calvo[48] (see also Ref. 28) for the case of a spin (arbitrarily seated in site 1) weakly interacting with n_j neighbor spins j with equal exchange couplings $J_{1,j}$ [according Eq. (6)]:

$$\hbar^2\omega_{ex}^2 \approx \sum_j n_j |J_{1,j}|^2, \tag{19}$$

where the sum is over the spins j. Because of the second power in the couplings, and the fast exponential dependence of the exchange interaction with distance of $|J_{i,j}|$, only few terms have to be considered in the sum. Considering the discussion of the chemical paths for superexchange between dinuclear units in the crystallographic section, the main interaction of a given unit type A is with one unit type D, supported by a path having five diamagnetic, including one O···H-C hydrogen bond. Thus, for $Cu_2[TzTs]_4$ it is:

$$\hbar\omega_{ex} = |J_{AD}| = |J'|.$$

An average of the values of ω_{ex} obtained from Figs. 9 and 10 and given in Table II was obtained and allows us to conclude that $|J|=(0.060 \pm 0.015)$ cm^{-1}. The sign of J' cannot be obtained from our EPR results.

VI. DISCUSSION AND CONCLUSIONS

This work reports a detailed EPR study of powder and single-crystal samples of $Cu_2[TzTs]_4$. This compound contains noncentrosymmetric copper(II) dinuclear units, with copper ions Cu^1 and Cu^2 bridged by four bidentate sulphathiazolato anions Cu^1-N-C-N-Cu^2. The exchange coupling between coppers in the dinuclear unit calculated from the temperature variation of the intensity of the powder EPR spectrum $J_0=(-113 \pm 1)$ cm^{-1} is antiferromagnetic and compares well with the values $J_0=-121.3$ and -104.3 cm^{-1} obtained for two compounds with similar nonlinear triatomic-N-C-N-bridges.[41] We also evaluated $D=(0.198 \pm 0.003)$ cm^{-1} and $E \sim 0$ for the principal values of the zero-field splitting of the $S=1$ triplet state arising from the dinuclear unit. They are related to the principal values $D=\mathcal{D}/4$ and $E=\mathcal{E}/4$ of the intradinuclear anisotropic spin-spin interaction of Eq. (4) [compare Eqs. (13) and (14)]. The main source of this interaction is the dipolar coupling between the two copper ions at 2.786 Å in the dinuclear units

that amounts more than 75% of the coupling, as calculated with the point-dipole approximation.

The most interesting finding of our work is the observation of the collapse of the structure of the EPR spectrum arising from the anisotropic spin-spin coupling between the copper ions, in a dinuclear unit. This phenomenon, which has not been observed before for dinuclear (or polynuclear) clusters of electronic spins, is attributed to the exchange couplings between a given dinuclear unit and the environment of other neighbor dinuclear units in the lattice. These provide a stochastic interaction capable of averaging out the dipolar coupling when the weak random interaction is larger than the anisotropic intradinuclear coupling. In that situation a sudden phase transition occurs and the coupling with the environment leads to decoherence, a quantum phase transition that collapses the dipolar interaction. Our EPR experiments in single-crystal samples provide a procedure to follow the classical exchange-narrowing process as a shift and collapse of the line structure (not as a variation of the resonance width), which is described using results of general theories of magnetic resonance and Anderson's and Kubo's models for exchange narrowing.[3–7] We cannot explain the differences between the values of $\hbar\omega_{ex}$ [Eq. (11)] obtained from line shift and from line-width measurements; a mean value of ω_{ex} was then used to calculate the exchange couplings. A simple analysis of the observed collapse allows us to estimate the magnitude of the exchange couplings between neighbor dinuclear units. In summary, using complementary procedures, our EPR measurements in powder and single-crystal samples allow us measuring three types of interactions differing by more than three orders of magnitude.

The average value estimated for the exchange coupling $|J'|=(0.060 \pm 0.015)$ cm^{-1} between a dinuclear unit and the nearest-neighbor dinuclear units is assigned to a chemical path containing five diamagnetic atoms, including a weak O···H-C hydrogen bond. This path connects translated Cu ions in different units through their apical oxygen ligands. The two conditions, a H bond in the path and the apical bonds to the copper ions, make the coupling necessarily weak. This value of $|J'|$ has a magnitude compatible with what was obtained for similar contacts between Cu in copper-amino acid and copper-peptide compounds[26–28,50–54] and in metaloproteins.[55,56]

An important fact observed in the EPR spectra of the powder sample is a hyperfine splitting with seven components at or below 50 K [see Fig. 3(b), B_{z1} component]. This multiplicity reinforces that it belongs to the spectrum of the dinuclear unit. We consider that when lowering the temperature, the population of the $S=1$ triplet state of the dinuclear unit decreases and as a consequence, decreases the magnitude of the exchange coupling between dinuclear units. At these temperatures the high-temperature approximation, usually made in the statistical calculations, is not valid for the dinuclear unit. The higher resolution of the hyperfine coupling at lower T is produced by a decrease of the interdinuclear interaction where the magnetic triplet state is depopulated.

Recently, Sebastian and coworkers[57,58] studied magnetic properties and EPR spectra of the compound $BaCuSi_2O_6$ having copper(II) ions in dinuclear units, as a function of

temperature at EPR frequencies between 26 and 660 GHz. The focus of their EPR work,[58] performed in a single crystal at only two magnetic-field orientations, is different than ours. In the low T region, where they obtain most of the data, the interdinuclear exchange is quenched by the depopulation of the triplet state. At these temperatures the mononuclear Cu(II) contaminant is the most important contributor to their EPR spectra, and where the upsurge of the hyperfine coupling (four peaks) appears when lowering T. These results point to the role of the interdinuclear exchange interactions, as our work does. We consider, however, that our more detailed single-crystal experiments performed at higher temperatures provide a better view of the role of the interdinuclear interactions, and also about the basic exchange-narrowing phenomenon. As mentioned above, we observe in a powder sample, below 50 K, an upsurge of hyperfine coupling, but, instead of that of the minority mononuclear species, that of the main dinuclear component [see resonance B_{z1} in Fig. 3(b)]. In addition we clearly follow the collapse of the structure arising from the intradinuclear dipolar interactions.

The purpose of this paper was measuring exchange coupling between the magnetic molecules from single-crystal EPR measurements in a polynuclear metal compound. These interactions may be responsible of spin-spin relaxation, a property important for the behavior of single-molecule magnets. Along these measurements we observed a new quantum mesoscopic effect in electronic spins, and evaluated very weak exchange couplings, using a simple theoretical analysis. More elaborate versions of the Anderson–Kubo theories[15] are not needed for the basic interpretation of our results for $Cu_2[TzTs]_4$ shown in Figs. 3(b) and 8–10. At this moment we are performing further experimental and theoretical works which may promote experimental progresses in the problem, and studies of more complex polynuclear magnetic entities.

ACKNOWLEDGMENTS

*Corresponding author. ciro@if.sc.usp.br. FAX: +55-16-3371-5381.

[1] C. J. Gorter and J. H. Van Vleck, Phys. Rev. **72**, 1128 (1947).

[2] J. H. Van Vleck, Phys. Rev. **74**, 1168 (1948).

[3] P. W. Anderson and P. R. Weiss, Rev. Mod. Phys. **25**, 269 (1953).

[4] P. W. Anderson, J. Phys. Soc. Jpn. **9**, 316 (1954).

[5] R. Kubo and K. Tomita, J. Phys. Soc. Jpn. **9**, 888 (1954).

[6] R. Kubo, in *Fluctuation, Relaxation, and Resonance in Magnetic Systems*, edited by D. Ter Haar (Oliver and Boyd, Edinburgh, 1962), p. 23.

[7] R. Kubo, in *Stochastic Processes in Chemical Physics*, Advances in Chemical Physics Vol. XV, edited by K. E. Schuler (Wiley, New York, 1969), p. 101.

[8] A. Abragam, *The Principles of Nuclear Magnetism* (Clarendon, Oxford, 1961).

[9] G. E. Pake, *Paramagnetic Resonance, an Introductory Monograph* (Benjamin, New York, 1962).

[10] A. Abragam and B. Bleaney, *Electron Paramagnetic Resonance of Transition Ions* (Clarendon, Oxford, 1970).

[11] J. R. Pilbrow, *Transition Ion Electron Paramagnetic Resonance* (Clarendon, Oxford, England, 1990).

[12] A. Bencini and D. Gatteschi, *Electron Paramagnetic Resonance of Exchange Coupled Systems* (Springer-Verlag, Berlin, NY, 1990).

[13] N. M. Atherton, *Principles of Electron Spin Resonance* (Ellis Horwood, Chichester/Prentice-Hall, New York, 1993).

[14] J. A. Weil, J. R. Bolton, and J. E. Wertz, *Electron Paramagnetic Resonance: Elementary Theory and Practical Applications* (Wiley, New York, 1994).

[15] Y. Tanimura, J. Phys. Soc. Jpn. **75**, 082001 (2006).

[16] B. Bleaney and K. D. Bowers, Proc. R. Soc. London **214**, 451 (1952).

[17] O. Kahn, *Molecular Magnetism* (VCH, New York, 1993).

[18] M. Verdaguer, Polyhedron **20**, 1115 (2001).

[19] E. I. Solomon and D. E. Wilcox, in *Magneto Structural Correlations in Exchange Coupled Systems*, edited by R. D. Willet, D. Gatteschi, and O. Kahn (Reidel, Dordrecht, 1985), p. 463.

[20] R. H. Holm, P. Kennepohl, and E. I. Solomon, Chem. Rev. (Washington, D.C.) **96**, 2239 (1996).

[21] E. I. Solomon, U. M. Sundaram, and T. E. Machonkin, Chem. Rev. (Washington, D.C.) **96**, 2563 (1996).

[22] C. J. OConnor, Prog. Inorg. Chem. **29**, 203 (1982).

[23] S. Cabaleiro, R. Calvo, J. Castro, J. A. García-Vázquez, L. M. B. Napolitano, O. R. Nascimento, P. Pérez-Lourido, J. Romero, and A. Sousa, J. Chem. Cryst. **38**, 71 (2008).

[24] R. Kubo, M. Toda, and N. Hashitsume, *Statistical Physics II: Nonequilibrium Statistical Mechanics* (Springer-Verlag, Berlin, 1991).

[25] S. Sachdev, *Quantum Phase Transitions* (Cambridge University Press, Cambridge, NY, 1999).

[26] D. M. Martino, M. C. G. Passeggi, and R. Calvo, Phys. Rev. B **52**, 9466 (1995).

[27] D. M. Martino, M. C. G. Passeggi, R. Calvo, and O. R. Nascimento, Physica B (Amsterdam) **225**, 63 (1996).

[28] R. Calvo, Appl. Magn. Reson. **31**, 271 (2007).

[29] Reference 6 describes results of papers where similar experiments with nuclear spins were reported.

[30] P. R. Levstein, G. Usaj, and H. M. Pastawski, J. Chem. Phys. **108**, 2718 (1998).

[31] G. A. Alvarez, E. P. Danieli, P. R. Levstein, and H. M. Pastawski, J. Chem. Phys. **124**, 194507 (2006).

[32] H. M. Pastawski, Physica B **398**, 278 (2007).

[33] W. Wernsdorfer, N. Aliaga-Alcalde, D. N. Hendrickson, and G. Christou, Nature (London) **416**, 406 (2002).

[34] W. Wernsdorfer, S. Bhaduri, R. Tiron, D. N. Hendrickson, and G. Christou, Phys. Rev. Lett. **89**, 197201 (2002).

[35] S. Hill, R. S. Edwards, N. Aliaga-Alcalde, and G. Christou, Science **302**, 1015 (2003).

[36] B. Barbara, Nature (London) **421**, 32 (2003).

[37] L. J. Farrugia, J. Appl. Crystallogr. **30**, 565 (1997).

[38] A. J. Arduengo, S. F. Gamper, M. Tamm, J. C. Calabrese, F. Davidson, and H. A. Craig, J. Am. Chem. Soc. **117**, 572 (1995).

[39] J. A. Platts, S. T. Howard, and K. Wozniak, Chem. Commun. (Cambridge) **1996**, 63.

[40] T. Steiner, Angew. Chem., Int. Ed. **41**, 48 (2002).

[41] R. Cejudo-Marín, G. Alzuet, S. Ferrer, J. Borrás, A. Castiñeiras, E. Monzani, and L. Casella, Inorg. Chem. **43**, 6805 (2004).

[42] A. J. Costa-Filho, C. E. Munte, C. Barberato, E. E. Castellano, M. P. D. Mattioli, R. Calvo, and O. R. Nascimento, Inorg. Chem. **38**, 4413 (1999).

[43] S. Stoll and A. Schweiger, J. Magn. Reson. **178**, 42 (2006).

[44] MATLAB, The MathWorks, Inc., Natick, MA 01760.

[45] J. A. Weil, EPR Newsletter **17**, 13 (2007).

[46] S. Stoll (private communication).

[47] P. R. Levstein and R. Calvo, Inorg. Chem. **29**, 1581 (1990).

[48] M. C. G. Passeggi and R. Calvo, J. Magn. Reson., Ser. A **114**, 1 (1995).

[49] C. D. Brondino, N. M. C. Casado, M. C. G. Passeggi, and R. Calvo, Inorg. Chem. **32**, 2078 (1993).

[50] A. J. Costa-Filho, O. R. Nascimento, L. Ghivelder, and R. Calvo, J. Phys. Chem. B **105**, 5039 (2001).

[51] A. J. Costa-Filho, O. R. Nascimento, and R. Calvo, J. Phys. Chem. B **108**, 9549 (2004).

[52] R. C. Santana, R. O. Cunha, J. F. Carvalho, I. Vencato, and R. Calvo, J. Inorg. Biochem. **99**, 415 (2005).

[53] E. D. Vieira, N. M. C. Casado, G. Facchin, M. H. Torre, A. J. Costa, and R. Calvo, Inorg. Chem. **45**, 2942 (2006).

[54] E. F. Chagas, R. E. Rapp, D. E. Rodrigues, N. M. C. Casado, and R. Calvo, J. Phys. Chem. B **110**, 8052 (2006).

[55] R. Calvo, E. C. Abresch, R. Bittl, G. Feher, W. Hofbauer, R. A. Isaacson, W. Lubitz, M. Y. Okamura, and M. L. Paddock, J. Am. Chem. Soc. **122**, 7327 (2000).

[56] R. Calvo, R. A. Isaacson, M. L. Paddock, E. C. Abresch, M. Y. Okamura, A. L. Maniero, L. C. Brunel, and G. Feher, J. Phys. Chem. B **105**, 4053 (2001).

[57] S. E. Sebastian, N. Harrison, C. D. Batista, L. Balicas, M. Jaime, P. A. Sharma, N. Kawashima, and I. R. Fisher, Nature (London) **441**, 617 (2006).

[58] S. E. Sebastian, P. Tanedo, P. A. Goddard, S. C. Lee, A. Wilson, S. Kim, S. Cox, R. D. McDonald, S. Hill, N. Harrison, C. D. Batista, and I. R. Fisher, Phys. Rev. B **74**, 180401(R) (2006).

[59] F. H. Allen, Acta Crystallogr., Sect. B: Struct. Sci. **58**, 380 (2002).

[60] I. J. Bruno, J. C. Cole, P. R. Edgington, M. Kessler, C. F. Macrae, P. McCabe, J. Pearson, and R. Taylor, Acta Crystallogr., Sect. B: Struct. Sci. **58**, 389 (2002).